Inter Coupling Modes Determination in Double Screen Frequency Selective Surfaces using the WCIP Method for Optimized Strip Length by Applying Real Genetic Algorithm

Asma Bounouara
Electronic Department, Faculty of Technology, University of Batna 2, Algeria
as.bounouara@univ-batna2.dz (corresponding author)

Mohammed Titaouine
Electronic Department, Faculty of Technology, University of Batna 2, Algeria
m.titaouine@univ-batna2.dz

Received: 17 March 2025 | Revised: 4 April 2025 and 10 April 2025 | Accepted: 12 April 2025

 DOI: https://doi.org/10.48084/etasr.11002

ABSTRACT

This paper presents a novel approach based on optimizing the strip length of a Frequency Selective Surface (FSS) structure using a Real Genetic Algorithm (RAG) in conjunction with the Wave Concept Iterative Method (WCIP). Mean Squared Error (MSE) is used as an objective function to calculate the error between the desired resonant frequency and the estimated one obtained through WCIP for each individual within the population. The approach was validated on two strip FSS structures, FSS_1 and FSS_2, showing a remarkable accuracy with relative errors of 0.0033% and 0.0029%, respectively. The results were obtained using MATLAB. After optimizing the length strips of both FSSs and cascading them, a strategy for identifying the coupling modes between the resulting double-screen FSS structure is introduced. The extracted coupling modes indicate that increasing the separation distance between the two FSSs reduces the number of modes participating in the coupling between FSS_1 and FSS_2. Two inter-FSS distance tests were used to validate the inter-FSS coupling modes determination strategy, and a good agreement was recorded between all mode WCIP results and the limited coupling mode WCIP results.

Keywords-FSS; real genetic algorithm; coupling modes; full-wave WCIP method

I. INTRODUCTION

Frequency Selective Surfaces (FSSs) are fundamental electromagnetic filters in microwaves. FSSs have been the subject of extensive studies in recent years because they find numerous applications in both the commercial and military sectors to supply multiple frequency band operations [1-3]. Strip length FSS optimization using RGA involves adjusting the geometric parameters to achieve specific electromagnetic performance, such as resonant frequency, bandwidth, or polarization behavior [4]. The Genetic Algorithm (GA) is a search heuristic of stochastic global optimization methods based on genetic recombination and the theory of natural evolution [5-6]. After optimizing the length strips of both FSSs and cascading them, a strategy for identifying the coupling modes between the double screen FSSs structure is introduced. A double-screen FSS is a structure composed of multiple layers of periodic elements designed to control electromagnetic wave propagation [7]. The coupling between two FSSs is an important topic in electromagnetic engineering, particularly in the design of filters. It involves the interaction of electromagnetic waves between two closely spaced or interacting FSS structures, leading to changes in transmission, reflection, and resonance properties [7].

Determining the FSS strip length is considered an optimization problem in the first part of this study. The objective is to optimize the strip length of the FSS unit cell to achieve the desired frequency response using RGA in conjunction with the WCIP method. The comparison of the obtained to the desired results is extremely close, with a relative error of less than 1%. The second part is based on the study of the modes involved in the coupling between the two-layer FSSs. This study demonstrates that the increased separation distance between FSSs decreased the number of intermodes involved in the coupling between FSS_1 and FSS_2.

II. REAL GENETIC ALGORITHM (RGA) OVERVIEW

This section supposes an RGA used to solve an optimization problem to determine the strip length in FSS, which usually refers to a GA that operates on continuous (real-valued) variables rather than binary variables [8]. In the

original simple GA, each individual is typically represented by a binary string (a series of 0 and 1), which can limit its application to problems where binary encoding is not optimal [9]. In contrast, an RGA directly represents individuals as real-valued vectors. This approach is particularly useful for optimization problems where variables naturally exist in a continuous space, with an objective function $f(x)$ where x is the optimized parameter. Figure 1 shows a flowchart of the RGA technique.

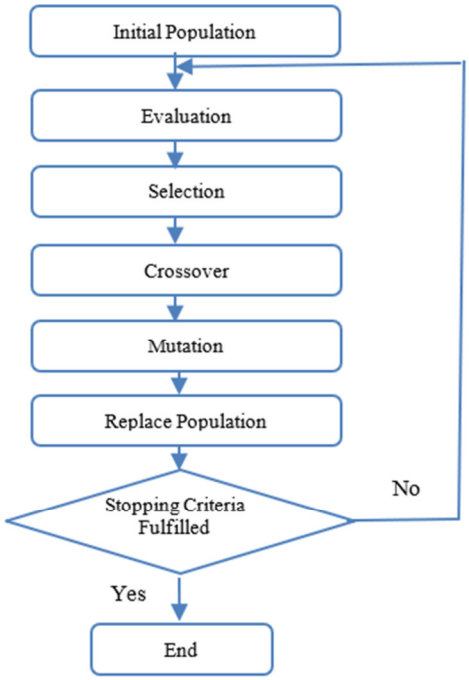

Fig. 1. Flowchart of RGA.

The process begins with a set of individuals called the initial population. RGA starts by constructing an initial population consisting of N individuals generated randomly within the search space [10]. The evaluation step is generally used to calculate each individual's fitness based on an objective function. In this work, the WCIP method is applied to obtain raw fitness scores. Then, the selection operator is a mechanism used to choose individuals from a population for reproduction, guiding the evolution process toward better solutions. The goal is to ensure that individuals with higher fitness have a greater chance of being selected to pass on their genes to the next generation. The crossover operator plays a central role in exploring the search space and combining the characteristics of parent solutions to create offspring, using real-number operators [11]. The mutation operator introduces diversity by modifying individual genes (real-valued parameters) in a solution. This prevents premature convergence and allows the exploration of new areas in the solution space of the offspring by adding small perturbations to their real-valued genes [11]. Finally, the replacement population decides which individuals will constitute the next generation. The elitist model is the most common strategy in the context of genetic algorithms. The primary objective is to avoid the convergence difficulty often associated with the loss of high-quality solutions due to random variations in the genetic operations of crossover and mutation [10]. The elitist strategy ensures that the best solutions are preserved over generations, preventing a decrease in the overall fitness of the population [10]. The iterative process of genetic operations continues until an acceptable optimum solution is found. This process involves repeated application of selection, crossover, mutation, and replacement to evolve the population over multiple generations.

III. THEORY OF DOUBLE SCREEN WCIP METHOD

To analyze the FSS structures with the WCIP method, they are simplified to a unit cell of the array enclosed by periodic walls. In addition, the dual-band FSSs can be designed by cascading double-screen FSS structures [12-13]. Figure 2 presents the two-level metallic strip FSS unit cell.

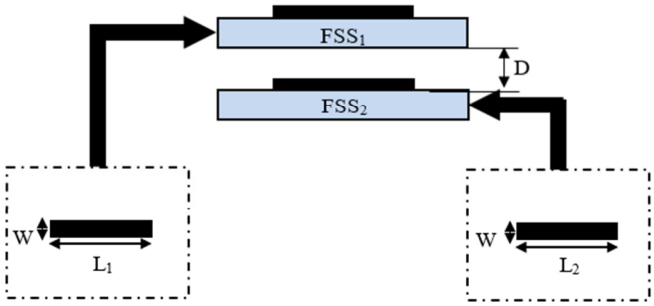

Fig. 2. Two-level metallic strip FSS unit cell.

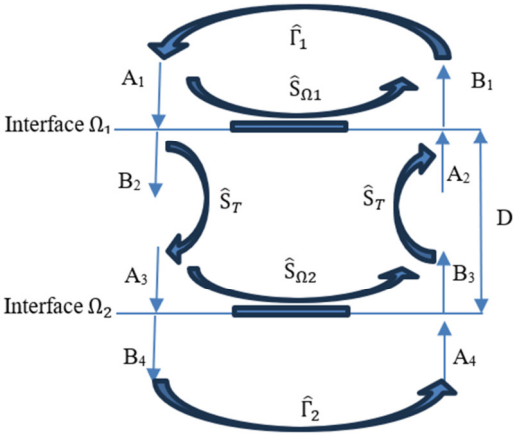

Fig. 3. Double screen WCIP method concept.

As shown in Figure 3, the diffracted waves $\vec{B}_i^{(k)}$ at the k^{th} iteration are acquired from the incident waves $\vec{A}_i^{(k)}$ [14]:

$$\vec{B}_i^{(k)} = \vec{S}_{\Omega i}\, \vec{A}_i^{(k)} \quad (1)$$

where $\vec{S}_{\Omega i}$ is the diffraction operator at the interface Ω_i containing the FSS circuit. This is defined in the spatial domain where $i = 1$ or 2 means FSS_1 or FSS_2, respectively, and it is determined from the geometric structure shape of the FSS unit cell and the limit conditions of each domain at the interface.

The diffracted waves are decomposed into the modal basis of a periodic rectangular waveguide, consisting of TEM, TE, and TM modes, forming a complete set. Each resulting mode propagates independently, remaining uncoupled in the modal domain. Consequently, each mode is reflected with its specific reflection coefficient [15].

The incident waves $\vec{A}_i^{(k+1)}$ of the $(k+1)^{th}$ iteration can be calculated from [14]:

$$\vec{A}_i^{(k+1)} = \hat{\Gamma}_i \, B_i^{(k)} + \vec{A}_0 \quad (2)$$

where $\hat{\Gamma}_i \, B_i^{(k)}$ determines the reflected waves of the k^{th} iteration, $\hat{\Gamma}_i$ is the reflection operator obtained in the modal domain of the medium i, and $\vec{A}_0$ is a wave source incident.

The Fast Modal Transform (FMT) pair FMT/FMT^{-1} switching between spatial and spectral domains is necessary at each iteration and is given in [14-17]:

$$B_{Modal} = FMT(B_{Spatial}) \quad (3)$$

$$B_{Spatial} = FMT^{-1}(B_{Modal}) \quad (4)$$

The iterative procedure of the full wave WCIP method is repeated until convergence of the input admittance Y_{in} is achieved. The full-wave WCIP method's convergence is assured due to the bounded reflection operator independent of the analyzed structure [15].

In the full-wave WCIP method, the distance separating two levels of metallic FSS structures is modeled by a transmission line of length D. Thus, a transition operator that relates the waves emitted from each side of the dielectric layer in the medium separating the two FSSs is introduced [18]:

$$\vec{A} = \hat{S}_T \, \vec{B} \quad (5)$$

The transition operator is given by [18]:

$$\left[\hat{S}_T^{\alpha}\right] = \begin{bmatrix} S_{11}^{\alpha} & S_{12}^{\alpha} \\ S_{21}^{\alpha} & S_{22}^{\alpha} \end{bmatrix} \quad (6)$$

with :

$$S_{11}^{\alpha} = S_{22}^{\alpha} = (Z_{\alpha}^2 - Z_{02}^2)\sinh(\gamma_{2m}D) \quad (7)$$

$$S_{12}^{\alpha} = S_{21}^{\alpha} = \frac{2Z_{\alpha}Z_{02}}{\Delta^2} \quad (8)$$

$$\Delta^{\alpha} = 2Z_{\alpha}Z_{02}\cosh(\gamma_{2,mn}D) + (Z_{\alpha}^2 + Z_{02}^2)\sinh(\gamma_{2,mn}D) \quad (9)$$

where α stands for the TE_{mn} or TM_{mn} modes, Z_{α} is the impedance of the mn^{th} TE mode or TM mode, Z_{02} is the characteristic impedance of the medium 2 separating the two interfaces Ω_1 and Ω_2, and $\gamma_{2,mn}$ is the propagation constant of the mn^{th} TE or TM mode in medium 2.

IV. APPLICATION OF RGA IN THE OPTIMIZATION OF STRIP LENGTH IN FSS

Two FSSs were chosen to illustrate the proposed approach's efficacy in determining the strip length to obtain the desired resonance frequencies $f_{r1} = 7$ GHz and $f_{r2} = 10.5$ GHz for FSS_1 and FSS_2, respectively. The geometrical dimensions of the FSS unit cell shown in Figure 4 have the following values: $a = b = 20$ mm, $W = 1$ mm, thickness of substrate $h = 1$ mm, electrical permittivity $\varepsilon_r = 4.4$, and L is the strip length to optimize.

The FSS structures are excited with x-polarized normal incident plane waves. Each FSS unit cell interface of Figure 4 is described by 100×100 pixels, and the WCIP iterative process stops after 350 iterations.

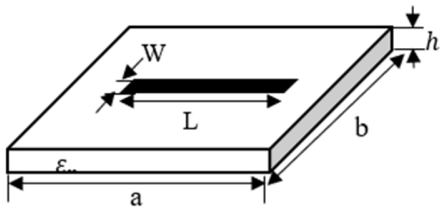

Fig. 4. Horizontal metallic strip FSS unit cell.

The object function is defined as an MSE error function between the desired transmission coefficient S_{21} and the estimated transmission coefficient $\hat{S}_{21}$ for each population of each generation as given by [19]:

$$MSE = \frac{1}{N}\sum_{i=1}^{N}(S_{21\,(i)} - \hat{S}_{21(i)})^2 \quad (10)$$

where N is the number of data points, $S_{21\,(i)}$ is the actual value for the i^{th} data point, and $\hat{S}_{21(i)}$ is the estimated value for the i^{th} data point.

The optimization parameters and the population size are chosen for the FSS case to be $N_{par} = 1$ and $N_{pop} = 20$, respectively. The convergence criterion is defined as $MSE \leq 10^{-9}$ and 100 generations. The search range of the optimization parameter is: 5 mm $\leq L \leq$ 16 mm.

The optimization process for FSS_1 and FSS_2 terminated after 32 and 21 generations, respectively, with an objective function value MSE of 1.025×10^{-9} and 2.49×10^{-7}. The optimized strip lengths of FSS_1 and FSS_2 are $L_1 = 14.033$ mm and $L_2 = 8.063$ mm, respectively. Figures 5 and 6 illustrate the results. The results indicate that the resonance frequency achieved after optimizing the strip length aligns with the desired cases of FSS_1 and FSS_2, presenting a good agreement with relative errors of 0.0033% and 0.0029%, respectively. The relative error is given by :

$$RelativeError = \frac{\|\hat{S}_{21} - S_{21\,desired}\|}{\|S_{21\,desired}\|} \quad (11)$$

with:

$$\|S_{21\,desired}\| = \sqrt{\sum_{j=1}^{M}\left[(S_{21\,desired})_j\right]^2} \quad (12)$$

$$\left\|S_{21\,desired} - \hat{S}_{21}\right\| = \sqrt{\sum_{j=1}^{M}\left[(S_{21\,desired})_j - \left(\hat{S}_{21}\right)_j\right]^2} \quad (13)$$

where M stands for the total number of frequencies, and $S_{21\,desired}$ and $\hat{S}_{21}$ are the desired and estimated values of transmission coefficients, respectively.

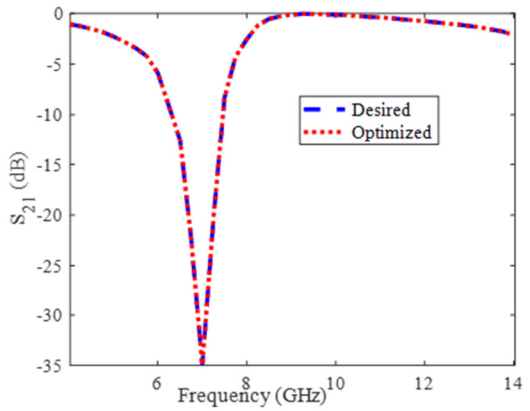

Fig. 5. Comparison between desired and optimized S_{21} of FSS_1.

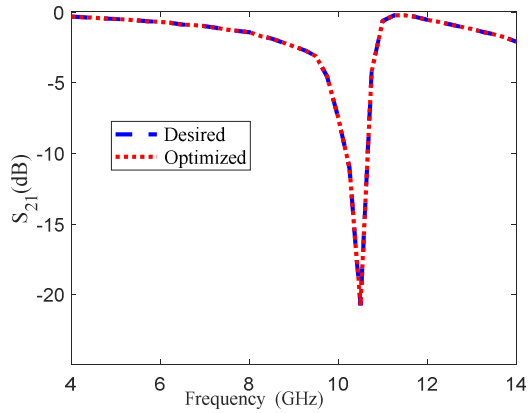

Fig. 6. Comparison between desired and optimized S_{21} of FSS_2.

V. INTER-FSS COUPLING MODES TYPE DETERMINATION STRATEGY

After optimizing the length strips of both FSSs and cascading them, the full-wave WCIP method is employed to examine the modes involved in the coupling between FSS_1 and FSS_2, and the results are presented in Table II. The separation distance D is presented in terms of the wavelength λ calculated by $\lambda = c/f$, where c is the constant of light given as $c = 3 \times 10^8$ m/s and f is the resonant frequency of the FSS_1 with $f_{r1} = 7 \text{ x}10^9$ Hz.

To begin the inter-FSS coupling mode determination process, the full-wave WCIP method, which includes all modes, is initially used as the reference, with 100 $TE_{m,n}$ modes and 100 $TM_{m,n}$ modes. Next, the WCIP method is applied with the TE and TM modes deleted, retaining only the fundamental TEM_x and TEM_y modes. The results from this approach are then compared to those obtained using the full-wave WCIP method with all modes included. If the relative error between the two results is less than 1%, it confirms that the coupling between FSS_1 and FSS_2 is insured by only the fundamental modes for a given separation distance D. A relative error in the optimization procedure of less than 1% provides an $\hat{S}_{21}$ shape extremely close to the full-wave WCIP S_{21} reference shape, as shown in Figures 4 and 5, with errors of 0.033% and 0.0029%, respectively, in the resonant frequency. The Specific Set of Modes (SSM) is to be determined from the different mode layers surrounding the fundamental mode and satisfying the condition of less than 1% relative error. The approach starts with the first layer of modes consisting of the first eight $TE_{m,n}$ and $TM_{m,n}$ modes surrounding the fundamental mode, where m and n range from -2 to 2. The obtained first layer SSM-WCIP results are compared with the reference case where all the modes are considered. If the relative error is less than 1%, the SSM mode with the lowest value from the transition operator elements S_{12}^{α} and S_{21}^{α} is deleted. This first layer process is repeated while the relative error remains below 1%. When the relative error exceeds 1%, the first layer SSM process is stopped, and the second layer SSM process is started with the first and second layers as the initial SSM modes. The flowchart of the SSM process is shown in Figure 7.

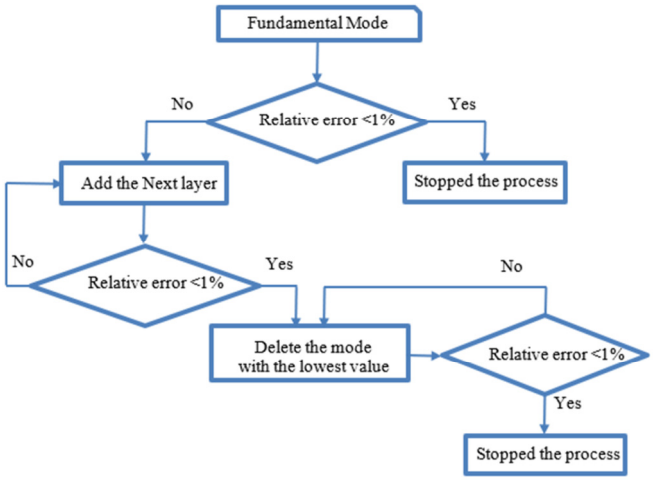

Fig. 7. Organization chart of the SSM process.

The final results concern the modes involved in the inter-FSS coupling as a function of the separation distance D, as shown in Table II.

The first layer ($1^{st}L$) modes consist of 8 TE modes and 8 TM, and the second layer ($2^{nd}L$) modes consist of 16 TE modes and 16 TM, as given in Table I.

TABLE I. MODES COMPONENT IN THE 1^{st} L AND 2^{nd} L

$1^{st}L$	$TE_{01}, TM_{01}, TE_{10}, TM_{10}, TE_{01}, TM_{01}, TE_{-10}, TM_{-10}, TE_{11}, TM_{11} TE_{-1-1}, TM_{-1-1}, TE_{-11}, TM_{-11}, TE_{1-1}, TM_{1-1}$.
$2^{nd}L$	$TE_{02}, TM_{02}, TE_{-20}, TM_{-20}, TE_{0-2}, TM_{0-2}, TE_{20}, TM_{20}, TE_{1-2}, TM_{1-2}, TE_{12}, TM_{12}, TE_{-12}, TM_{-12}, TE_{-1-2}, TM_{-2-1}, TE_{2-1}, TM_{2-1}, TE_{21}, TM_{21}, TE_{2-1}, TM_{2-1}, TE_{-21}, TM_{-21}, TE_{2-2}, TM_{2-2}, TE_{-2-2}, TM_{-2-2}, TE_{22}, TM_{22}, TE_{-22}, TM_{-22}$

Filling the layers begins by padding the first layer and then the second one, following the modes' order presented in Table I. Table II indicates that increasing the separation distance between the two FSSs reduces the number of modes participating in the coupling between the FSS_1 and FSS_2, as shown in Figure 8.

TABLE II. THE MODES INVOLVED IN THE COUPLING AS A FUNCTION OF THE SEPARATION DISTANCE D

$D\ (m)$	Modes involved in the coupling
$0.055 \times \lambda$	TE_{00} +TM_{00} +1^{st} L +2^{nd} L with deleted modes: TE_{2-2} , TM_{2-2} ,TE_{-2-2} , TM_{2-2} ,TE_{22} , TM_{22}, and TM_{-22} .
$0.06 \times \lambda$	TE_{00} +TM_{00} +1^{st} L +2^{nd} L with deleted modes: TE_{2-2} , TM_{2-2} ,TE_{-2-2} , TM_{2-2} ,TE_{22} , TM_{22} TE_{-22},TM_{-22}, and TM_{-21}
$0.065 \times \lambda$	TE_{00} +TM_{00} +1^{st} L +2^{nd} L with deleted modes: TE_{2-2} , TM_{2-2} ,TE_{-2-2} , TM_{2-2} ,TE_{22} , TM_{22} TE_{-22},TM_{-22} ,TE_{-21},TM_{-21}, and TM_{2-1}.
$0.07 \times \lambda$	TE_{00} +TM_{00} +1^{st} L +2^{nd} L with deleted modes : TE_{2-2} , TM_{2-2} ,TE_{-2-2} , TM_{2-2} ,TE_{22} , TM_{22} TE_{-22},TM_{-22} ,TE_{-21}, TM_{-21} ,TE_{2-1} .TM_{2-1} and TM_{21}.
$0.075 \times \lambda$	TE_{00} +TM_{00} +1^{st} L +2^{nd} L with deleted modes : TE_{2-2} , TM_{2-2} ,TE_{-2-2} , TM_{2-2} ,TE_{22} , TM_{22} TE_{-22},TM_{-22} ,TE_{-21},TM_{-21} ,TE_{2-1} .TM_{2-1},TE_{21} ,TM_{21}, and TM_{2-1}.
$0.08 \times \lambda$	TE_{00} +TM_{00} +1^{st} L + TE_{02}, TM_{02} ,TE_{-20} ,TM_{-20}, TE_{0-2} , TM_{0-2} and TE_{20} from the 2^{nd} L.
$0.085 \times \lambda$	TE_{00} +TM_{00} +1^{st} L + TE_{02}, TM_{02} ,TE_{-20} ,TM_{-20}, TE_{0-2} , TM_{0-2} and TE_{20} from the 2^{nd} L.
$0.09 \times \lambda$	TE_{00} +TM_{00} +1^{st} L + TE_{02}, TM_{02} and TE_{-20} from the 2^{nd} L
$0.095 \times \lambda$	TE_{00} +TM_{00} +1^{st} L + TE_{02} from the 2^{nd} L
$0.1 \times \lambda$	TE_{00} +TM_{00} +1^{st} L with deleted mode: TM_{1-1}
$0.15 \times \lambda$	TE_{00} +TM_{00} +1^{st} L with deleted modes: TE_{1-1}, TM_{1-1}, TE_{-11} ,TM_{-11} ,TE_{-1-1}, TM_{-1-1} , TE_{11}, TM_{11} , TM_{-10}
$0.2 \times \lambda$	TE_{00} +TM_{00} +1^{st} L with deleted modes :TE_{1-1}, TM_{1-1}, TE_{-11} ,TM_{-11} ,TE_{-1-1} ,TM_{-1-1} ,TE_{11} ,TM_{11}, and TM_{-10} .
$0.35 \times \lambda$	TE_{00} +TM_{00} +1^{st} L with deleted modes :TE_{1-1}, TM_{1-1}, TE_{-11} ,TM_{-11} ,TE_{-1-1} ,TM_{-1-1} ,TE_{11} ,TM_{11} and TM_{-10}.
$0.4 \times \lambda$	TE_{00} +TM_{00} +1^{st} L with deleted modes : TE_{1-1}, TM_{1-1}, TE_{-11} ,TM_{-11} ,TE_{-1-1} ,TM_{-1-1} ,TE_{11} ,TM_{11} and TM_{-10}.
$0.45 \times \lambda$	TE_{00}
$0.5 \times \lambda$	TE_{00}
$0.6 \times \lambda$	TE_{00}
$0.65 *\times \lambda$	TE_{00}
$0.7 \times \lambda$	TE_{00}

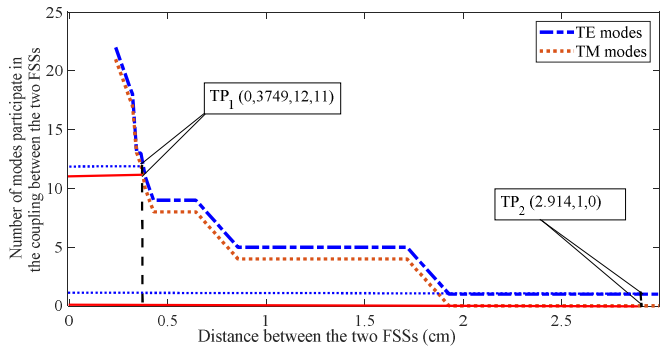

Fig. 8. Variation of the number of the modes involved in the coupling versus the FSSs' separation distance D.

Two Test Points TP(D, TE, TM) were chosen, as shown in Figure 8. TP_1 corresponds to the distance of 0.3749 cm between the two FSSs. According to Figure 8, the number of modes participating in the coupling between the two FSSs is 12 TE modes and 11 TM modes. SSM-WCIP is applied to the two screen FSSs of Figure 2 and the results are shown in Figure 9. A good agreement between the obtained results of SSM-WCIP and all WCIP mode results was recorded with a relative error of 0.9515%, which is less than 1% as apriori fixed.

The number of modes participating in the coupling between the two FSSs are only:

$TE_{00} + TM_{00} + 1^{st}L + TE_{02}$, TM_{02} , TE_{-20} , TM_{-20} , TE_{0-2}, TM_{0-2}, and TE_{20} from the $2^{nd}L$

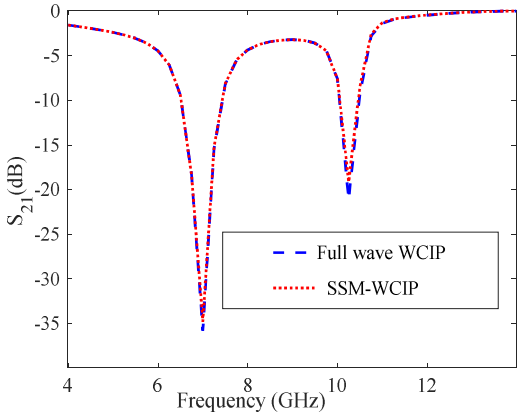

Fig. 9. Comparison between the frequency response of full-wave WCIP method and SSM-WCIP.

The later TP_2 coordinates are an inter-FSS distance of 2.914 cm and only one coupling mode is the TE_{00} mode. The application of the WCIP method with only TE_{00} mode leads to a transmission coefficient as shown in Figure 10. A good agreement between the obtained results is recorded with a relative error of 0.2658%, which is less than the maximum allowed error of 1%.

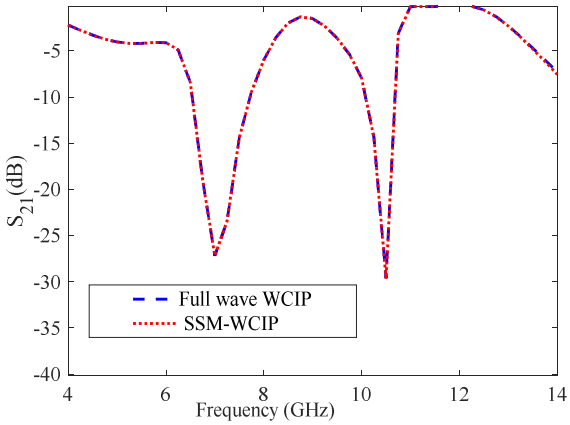

Fig. 10. Comparison between the frequency response of full0wave WCIP method and SSM-WCIP.

VI. CONCLUSION

This study proposes two novel approaches. The former deals with the optimization of the strip FSS length using RGA in conjunction with the WCIP method to achieve the desired resonance frequency. Two strip FSS lengths are optimized using RGA-WCIP and a good agreement between the desired and the optimized resonant frequencies is recorded within a relative error of less than 1%. The latter concerns the identification of the inter-coupling modes between the double screen FSS structure by introducing the SSM-WCIP strategy and the full wave WCIP method after optimizing the FSS strips

lengths using the RGA-WCIP approach. A list of the modes involved in the coupling between the double-screen FSS is determined for each inter-FSS separation distance. As the inter-FSS separation distance increases, the number of the involved coupling modes decreases, as can be concluded when the identified list of the involved coupling modes is observed. Two test points were chosen to validate the novel SSM-WCIP proposed strategy, and a good agreement in the allowed error of 1% was observed between the SSM-WCIP results and the full-wave WCIP results. The identified inter-FSS coupling mode list can serve as a reference when the inter-double-screen FSS coupling modes need to be known for a specific inter-FSS separation distance.

REFERENCES

[1] R. Saidi *et al.*, "Characterization of Switchable Rectangular Ring FSS with Non Coupled Parallel Metallic Strips for Multi Band and Dual Polarized Applications Using WCIP Method," *Journal of Microwaves, Optoelectronics and Electromagnetic Applications*, vol. 17, no. 1, pp. 102–120, Mar. 2018, https://doi.org/10.1590/2179-10742018v17i11057.

[2] G. Manara, A. Monorchio, and R. Mittra, "Frequency selective surface design based on genetic algorithm," *Electronics Letters*, vol. 35, no. 17, pp. 1400–1401, Aug. 1999, https://doi.org/10.1049/el:19990991.

[3] S. Chakravarty, R. Mittra, and N. R. Williams, "On the application of the microgenetic algorithm to the design of broad-band microwave absorbers comprising frequency-selective surfaces embedded in multilayered dielectric media," *IEEE Transactions on Microwave Theory and Techniques*, vol. 49, no. 6, pp. 1050–1059, Jun. 2001, https://doi.org/10.1109/22.925490.

[4] A. Bounouara, M. Titaouine, K. Bencherif, and R. Saidi, "Optimization of Strips Lengths in Parallel Non Coupled Metallic Strips Frequency Selective Surfaces (FSS) Using Genetic Algorithm (GA) and WCIP Method," in *Proceedings of the 5th International Conference on Electrical Engineering and Control Applications–Volume 2*, 2024, pp. 317–325, https://doi.org/10.1007/978-981-97-4776-4_32.

[5] H. O. Aljorany and A. M. R. Mahjoob, "Establishing a Budget for Optimal Response Strategies for Risks Categorized into Distinct Groups by using a Mathematical Model and Genetic Algorithm," *Engineering, Technology & Applied Science Research*, vol. 14, no. 3, pp. 14747–14753, Jun. 2024, https://doi.org/10.48084/etasr.7526.

[6] D. E. Goldberg, *Genetic Algorithms in Search, Optimization and Machine Learning*, 1st ed. Boston, MA, USA: Addison-Wesley Professional, 1989.

[7] W. Afzal, M. Z. Baig, A. Ebrahimi, M. R. Robel, M. T. A. Rana, and W. Rowe, "Frequency Selective Surfaces: Design, Analysis, and Applications," *Telecom*, vol. 5, no. 4, pp. 1102–1128, Dec. 2024, https://doi.org/10.3390/telecom5040056.

[8] A. Qing, C. K. Lee, and L. Jen, "Microwave Imaging of Parallel Perfectly Conducting Cylinders Using Real-Coded Genetic Algorithm," *Journal of Electromagnetic Waves and Applications*, vol. 13, no. 8, pp. 1121–1143, Jan. 1999, https://doi.org/10.1163/156939399X01276.

[9] A. Qing, C. K. Lee, and L. Jen, "Electromagnetic inverse scattering of two-dimensional perfectly conducting objects by real-coded genetic algorithm," *IEEE Transactions on Geoscience and Remote Sensing*, vol. 39, no. 3, pp. 665–676, Mar. 2001, https://doi.org/10.1109/36.911123.

[10] X. F. Luo, A. Qin, and C. K. Lee, "The design of frequency selective surfaces (FSS) using real-coded genetic algorithm (RGA)," in *Fourth International Conference on Information, Communications and Signal Processing, 2003 and the Fourth Pacific Rim Conference on Multimedia. Proceedings of the 2003 Joint*, Singapore, 2003, vol. 1, pp. 391–395, https://doi.org/10.1109/ICICS.2003.1292481.

[11] Z. Michalewicz, *Genetic Algorithms + Data Structures = Evolution Programs*. Springer Science & Business Media, 2013.

[12] M. Al-Joumayly and N. Behdad, "A New Technique for Design of Low-Profile, Second-Order, Bandpass Frequency Selective Surfaces," *IEEE Transactions on Antennas and Propagation*, vol. 57, no. 2, pp. 452–459, Oct. 2009, https://doi.org/10.1109/TAP.2008.2011382.

[13] M. Yan *et al.*, "A Miniaturized Dual-Band FSS With Second-Order Response and Large Band Separation," *IEEE Antennas and Wireless Propagation Letters*, vol. 14, pp. 1602–1605, 2015, https://doi.org/10.1109/LAWP.2015.2413942.

[14] S. Akatimagool, "Electromagnetic Software Tools for Microwave Multi-layer Integrated Circuits and Components," vol. 13, no. 2, 2003.

[15] K. Bencherif *et al.*, "Multiband FSS Analysis and Synthesis Based on Parallel Non Coupled Metallic Strips Using WCIP Method," *Journal of Microwaves, Optoelectronics and Electromagnetic Applications*, vol. 17, no. 4, pp. 433–456, Oct. 2018, https://doi.org/10.1590/2179-10742018v17i41264.

[16] S. Aroussi, L. Latrach, N. Sboui, A. Gharsallah, A. Gharbi, and H. Baudrand, "Efficient Analysis of Complex FSS Structure Using the WCIP Method," *Journal of Electromagnetic Analysis and Applications*, vol. 3, no. 11, pp. 447–451, Nov. 2011, https://doi.org/10.4236/jemaa.2011.311071.

[17] M. Titaouine, A. G. Neto, H. Baudrand, and F. Djahli, "Analysis of shorted ring slots frequency selective surfaces using WCIP method," *Journal of Microwaves, Optoelectronics and Electromagnetic Applications (JMOe)*, vol. 7, no. 2, pp. 65–82, 2008.

[18] M. Titaouine, N. Raveu, A. Gomes Neto, and H. Baudrand, "Dual-band and enhanced band FSS characterization using WCIP method," *Microwave and Optical Technology Letters*, vol. 52, no. 4, pp. 836–839, 2010, https://doi.org/10.1002/mop.25073.

[19] T. O. Hodson, T. M. Over, and S. S. Foks, "Mean Squared Error, Deconstructed," *Journal of Advances in Modeling Earth Systems*, vol. 13, no. 12, 2021, Art. no. e2021MS002681, https://doi.org/10.1029/2021MS002681.